RSC Advances

PAPER

View Article Online
View Journal | View Issue

Cite this: *RSC Adv.*, 2019, **9**, 5530

Large magnetocaloric effect in manganese perovskite $La_{0.67-x}Bi_xBa_{0.33}MnO_3$ near room temperature

Ah. Dhahri, *[ab] E. Dhahri [a] and E. K. Hlil[c]

$La_{0.67-x}Bi_xBa_{0.33}MnO_3$ (x = 0 and 0.05) ceramics were prepared *via* the sol–gel method. Structural, magnetic and magnetocaloric effects have been systematically studied. X-ray diffraction shows that all the compounds crystallize in the rhombohedral structure with the $R\bar{3}c$ space group. By analyzing the field and temperature dependence of magnetization, it is observed that both samples undergo a second order magnetic phase transition near T_C. The value of T_C decreases from 340 K to 306 K when increasing x from 0.00 to 0.05, respectively. The reported magnetic entropy change for both samples was considerably remarkable and equal to 5.8 J kg^{-1} K^{-1} for x = 0.00 and 7.3 J kg^{-1} K^{-1} for x = 0.05, respectively, for $\mu_0 H$ = 5 T, confirming that these materials are promising candidates for magnetic refrigeration applications. The mean-field theory was used to study the magnetocaloric effect within the thermodynamics of the model. Satisfactory agreement between experimental data and the mean-field theory has been found.

Received 28th November 2018
Accepted 30th January 2019

DOI: 10.1039/c8ra09802f

rsc.li/rsc-advances

1 Introduction

Over the past few years, the perovskite manganites with ABO_3-type compounds $Tr_{1-x}M_xMnO_3$ (where Tr stands for a trivalent rare-earth element such as Bi^{3+}, La^{3+} or Pr^{3+}, and M for the divalent alkaline earth ions such as Sr^{2+}, Ca^{2+} or Ba^{2+}), have been extensively studied due to their extraordinary magnetic and electronic properties as well as their promise for potential technological applications.[1,2] A prominent feature of the mixed-valence perovskite manganite materials is an insulator–metal (IM) transition accompanied simultaneously by the paramagnetic–ferromagnetic (PM–FM) transition giving rise to a colossal magnetoresistance (CMR) effect.[3] The existence of the observed CMR near the transition temperature was due to the mixed valence state of Mn, evolving from Mn^{3+} ($t_{2g}^3\uparrow e_g^1\uparrow$, $S = 2$) in the parent atom $LaMnO_3$ to Mn^{4+} ($t_{2g}^3\uparrow e_g^0$, $S = 3/2$) to the doped element $SrMnO_3$.[4] The double exchange interaction of the neighboring spin moment of (Mn^{3+}, Mn^{4+}) coupled through oxygen ions (O^{2+}), the small polaron theory and the Jahn–Teller (JT) effect have been proposed to explain the CMR phenomenon near the transition temperature.[5] In addition, when a field is applied to this material, the unpaired spins are aligned parallel to the field. Since the total entropy of spins plus the lattice remains constant, the magnetic entropy change ($-\Delta S_M$) is removed from the spin system and goes into the lattice, which lowers the magnetic entropy and produces a net heat. On the contrary, when an applied field is removed from a magnetic sample, the spin tends to become random, leading to increment of the entropy and causing the material to cool down. As well known, the maximum of the magnetic entropy change in this kind of material always occurs around its magnetic ordering temperature (*i.e.*, Curie temperature, T_C). Nowadays, there is a need of new advanced magnetics materials with a second order magnetic phase transition, showing a large reversible ($-\Delta S_M$) at low applied fields. Some theoretical works have focused on this subject, for second order phase transition *via* the molecular mean field theory.[6] For this it is important to know the field dependence of a given magnetic refrigerant sample. The study of the magnetocaloric effect is not only important from the point of view of potential applications; it also provides a tool to understand the intrinsic properties of a material. In Bi based manganites, the lone pair electrons of Bi^{3+} ion hybridize with oxygen 2p orbitals, which in turn reduces the bond length of d_{Bi-O} and bond angle of $\theta_{Mn-O-Mn}$ and increases the bond length of d_{Mn-O}.[7]

From this viewpoint, this paper reports the structural, magnetic and magnetic entropy change of Bi-substituted perovskite manganites $La_{0.62}Bi_{0.05}Ba_{0.33}MnO_3$. It is found that these materials show quite large magnetic entropy changes induced by low magnetic field changes.

2 Experimental details

Powders of $La_{0.67-x}Bi_xBa_{0.33}MnO_3$ (x = 0 and 0.05) were prepared *via* sol–gel route. In this process, $La(NO_3)_3\cdot 6H_2O$,

[a]Laboratoire de Physique Appliquée, Faculté des Sciences de Sfax, Université de Sfax, BP 1171, 3000, Tunisia. E-mail: dhahridhahri14@gmail.com; Tel: +216 20 20 45 55
[b]Faculté des Sciences de Monastir, Avenue de l'environnement 5019, Monastir, Tunisia
[c]Institut Néel, CNRS et Université J. Fourier, BP 166, 38042 Grenoble, France

$Ba(NO_3)_2$, $Bi(NO_3)_2 \cdot 5H_2O$ and $Mn(NO_3)_2 \cdot 6H_2O$ precursors, all with purity of 99.9%, were weighed in the desired proportions and dissolved with small amounts of water. Ethylene glycol (EG) and citric acid (CA) were used as polymerization/complexation agents, respectively, forming a stable solution. 100 cm^3 of metallic salts solution was added to 300 cm^3 of a solution containing a mixture of citric acid (60 g) and ethylene glycol (13 mL). This solution was then heated on a thermal plate under constant stirring, where polymerization occurs in the liquid solution and leads to a homogeneous sol. When the sol is further heated to remove the excess of solvent, an intermediate resin is formed. Calcination of the resin at 573 K in air was performed and sintering at 1073 K for 10 hours. These procedures are outlined in the flow chart of Fig. 1.

The phase purity and structure of sample were identified by X-ray powder diffraction at room temperature using a Siemens D5000 X-ray diffractometer with a graphite monochromatized CuKα radiation ($\lambda_{CuK\alpha} = 1.5406$ Å) and $20° \leq 2\theta \leq 90°$ with steps of 0.02° and a counting time of 18 s per step. According to our measurements, this system is able to detect up to a minimum of 3% of impurities. The structure analysis was carried out using the Rietveld method with FULLPROF software (version 0.2-Mars 1998-LLB-JRC).[8] Scanning electron microscopy (SEM) using a Philips XL30 equipped with a field emission gun at 20 kV was used to characterize $La_{0.67-x}Bi_xBa_{0.33}MnO_3$ morphologies.

Magnetization (M) *versus* temperature (T) and magnetization *versus* magnetic field ($\mu_0 H$) were performed by using BS1 and BS2 magnetometers developed in Louis Neel Laboratory at Grenoble. The isothermal curves were determined in the magnetic field range of 0–5 T. The temperature interval is fixed to 2 K in the vicinity of the Curie temperature (T_C). The temperature steps were smaller near T_C and larger further away.

3 Results and discussion

3.1 X-ray diffraction and microstructure analysis

The X-ray diffraction pattern for the samples ($x = 0.00$ and 0.05) is shown in Fig. 2. The samples of $La_{0.67-x}Bi_xBa_{0.33}MnO_3$ are a single phase without detectable secondary phase, within the

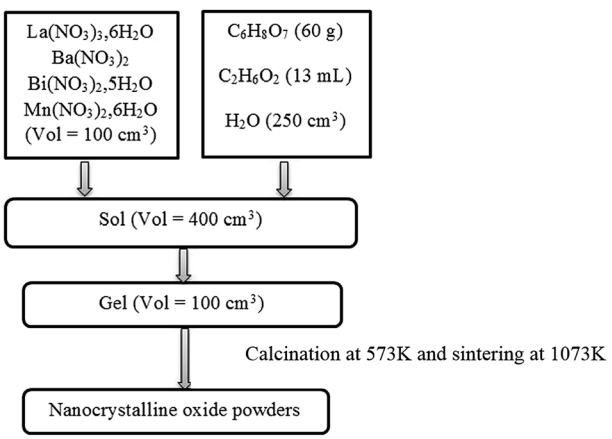

Fig. 1 A flow chart illustrating the processing procedure for $La_{0.67-x}Bi_xBa_{0.33}MnO_3$ powders preparation.

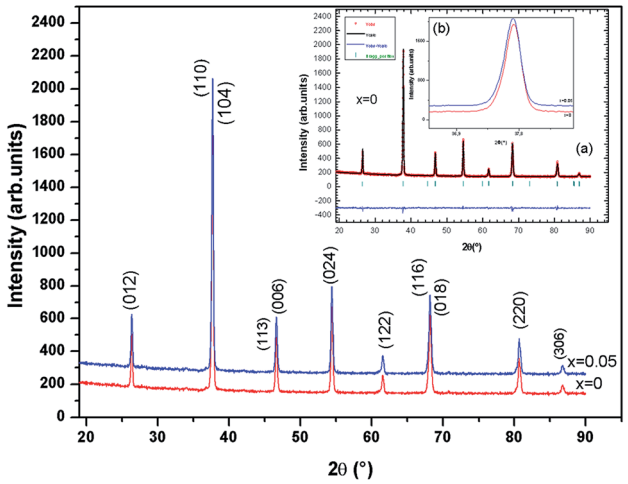

Fig. 2 X-ray powder diffraction patterns and Rietveld refinement for the compounds $La_{0.67-x}Bi_xBa_{0.33}MnO_3$ ($x = 0$ and 0.05) at room temperature.

sensitivity limits of the experiment (a few percent). The Rietveld refinements was successful considering the $R\bar{3}c$ (no. 167) rhombohedral and centro symmetric space group (inset (a) of Fig. 2, for $x = 0.0$ for example). Standard hexagonal setting of the $R\bar{3}c$ space group (with a_H and c_H cell parameters) was used. The manganite structure ($LaAlO_3$ type) is described in this hexagonal setting, with (La/Bi/Ba) atoms at 6a (0, 0, 1/4) position, Mn at 6b (0, 0, 0) and O at 18e (x, 0, 1/4) position. This distorted manganite is characterized by $\bar{a}\,\bar{a}\,\bar{a}$ antiphase oxygen octahedral tilt system (Glazer notation[9]) corresponding to rotations along the three pseudo cubic directions of the manganite. Detailed results of the structural refinements are regrouped in Table 1. It can be observed from the inset (b) in Fig. 2 that the position of the most intense peak shows a slight shift towards low angles with the increase of Bi, indicating that the cell volume of the $La_{0.67-x}Bi_xBa_{0.33}MnO_3$ specimens increases.

In order to quantitatively discuss the ionic match between A and B sites in perovskite compounds, a geometrical quantity, noted Goldschmidt tolerance factor (t), is usually introduced and is defined as:[10]

$$t = \frac{(r_{La+Bi+Ba} + r_O)}{\sqrt{2}(r_{Mn} + r_O)}$$

Here $r_{La+Bi+Ba}$; r_{Mn} and r_O are the average ionic radii of A, B and oxygen, respectively in the perovskite ABO_3 structure. Manganite compounds have a perovskite structure if their tolerance factor lies in the limits of $0.75 < t < 1$ and in an ideal case when the value must be equal to unity. In the present work, the tolerance factor of $La_{0.62}Bi_{0.05}Ba_{0.33}MnO_3$ is calculated from Shannon's ionic radii ($r_{La^{3+}} = 1.22$ Å, $r_{Bi^{3+}} = 1.24$ Å, $r_{Ba^{2+}} = 1.47$ Å, $r_{Mn^{3+}} = 0.645$ Å, $r_{Mn^{4+}} = 0.53$ Å, $r_{O^{2-}} = 1.35$ Å)[11,12] and it is found to be $t = 0.9595$ and 0.9599 for $x = 0$ and $x = 0.05$, respectively, which is within the range of stable perovskite structure.

The value of average crystallite size was estimated from the full width at half maximum (FWHM) of X-ray diffraction peaks.

Table 1 Physical properties of the sample $La_{1-x}Bi_xBa_{0.33}MnO_3$ system, prepared by sol–gel method at room temperature[a]

Crystallographic data			Refinement conditions				Average crystallite size			
Lattice parameters		Cell volume	Discrepancy factors							
$a = b$ (Å)	c (Å)	V (Å^3)	R_{wp} %	R_p %	R_F %	χ^2 %	Debye–Scherrer technique D_s (nm)	Williamson–Hall technique D_w (nm)	Strain ε (%)	Average grain size D (nm)
$x = 0$										
5.5160 (3)	13.5023(1)	355.78(2)	4.12	3.43	2.78	1.85	38	49	0.16	220
$x = 0.05$										
5.50184 (2)	13.5141(4)	356.40(1)	5.23	3.42	3.42	1.25	35	40	0.14	260

[a] a and c: hexagonal cell parameters; V: cell volume; R_{wp}, R_p; R_F: the residuals for, respectively, the weighted pattern, the pattern and the Bragg structure factor; χ^2: the goodness of fit. The numbers in parentheses are estimated standard deviations to the last significant digit.

The effects of synthesis, instruments and processing conditions were taken into consideration while making the calculation of crystallite size. The dependence of the size effect is given by Scherrer's formula: $\beta_{size} = \frac{K\lambda}{D_s \cos\theta}$, where λ is the wavelength of CuKα radiation ($\lambda = 1.5406$ Å), K is grain shape factor (=0.89) and D_s is the thickness of the crystal. Using the Williamson–Hall (W–H) method,[13] the average values of both D_w and lattice strain (ε) can be obtained from the intercept and the slope of the following relation, respectively,

$$\beta \cos\theta = \frac{K\lambda}{D_W} + 4\varepsilon \sin\theta$$

where β is the full-width at half-maximum of an XRD peak, θ is the Bragg angle, and $K = 0.9$ is the shape factor. The values of average crystallite size D_S, D_W and micro-strain of $La_{0.67-x}Bi_x$-$Ba_{0.33}MnO_3$ compounds are tabulated in Table 1. The particle size, calculated in the present system using Williamson–Hall technique, is larger than the particle size obtained from Debye–Scherrer method because the broadening effect due to strain is completely excluded in Debye–Scherrer technique.[14]

Fig. 3 shows the SEM photograph of the compounds. The samples contained connected particles with hexagonal shape and clear grain boundaries. These particles are largely agglomerated with a broad size distribution. The average value of thickness of both compounds is listed in Table 1.

After measuring the diameters of all the particles in SEM image, the size distribution histogram is fitted with the log-normal function expressed as:

$$f(D) = \left(\frac{1}{\sqrt{2\pi}\sigma D}\right) \exp\left[-\frac{\ln^2\left(\frac{D}{D_0}\right)}{2\sigma^2}\right]$$

Here D_0 and σ are the average diameter obtained from the SEM results and the data dispersions, respectively. The inset of Fig. 3 shows the dispersion histogram. The mean diameter $\langle D\rangle$ and standard deviation σ_D were determined using these relations:[15,16]

$$\langle D\rangle = D_0 \exp(\sigma^2/2)$$

$$\sigma_D = \langle D\rangle[\exp(\sigma^2) - 1]^{1/2}$$

The results analysis showed $\langle D\rangle \geq 397.48$ μm and $\sigma_D = 291.53$ μm.

3.2 Bulk magnetization

Low-field magnetization (M) *versus* temperature was first measured for the samples, in order to have an estimation of the transition temperature (T_C). The result is presented in Fig. 4. The $M(T)$ curve reveals that when increasing temperature, the samples exhibit a magnetic transition from paramagnetic (PM) state to ferromagnetic (FM) one. This transition occurs at the Curie temperature (T_C) which is obtained from the peak of dM/dT curve. The Curie temperature decreases from 340 K to 306 K when increase x from 0.00 to 0.05, respectively for $\mu_0 H = 0.05$ T. The Curie temperature of the Bi-doped compound was found to be lower than that of the undoped sample. This indicates that Bi substitution appears to weaken the magnetic interaction in the sample. Theoretical calculation has shown that off-center shifts of the ions with ns^2 electronic configuration results in the structural distortion and minimization of the Coulombic energy.[17] An orientation of the $6s^2$ lone pair toward a surrounding anion (O-2p) can produce a local distortion or even hybridization between Bi-6s-orbitals and O-2p orbitals,[18] leading to the block of the movement of e_g electrons through the Mn–O– Mn bridges (stronger localization).

The inset of Fig. 4 shows the temperature dependence of the inverse magnetic susceptibility of $x = 0$ and $x = 0.05$. It could be fitted to the Curie–Weiss law just above T_C (the PM region): $\chi = C/T - \theta_{CW}$, where θ_{CW} is the Weiss temperature and C is the Curie constant defined as: $C = \frac{\mu_0[g^2 J(J+1)\mu_B{}^2]}{3k_B} = \frac{\mu_0}{3k_B}\mu_{eff}{}^2$, where $\mu_0 = 10^7$ H m^{-1} is the permeability, g is the Landé factor, $\mu_B = 9.27 \times 10^{24}$ J T^{-1} is the Bohr magneton, $k_B = 1.38 \times 10^{23}$ J K^{-1} is the Boltzmann constant, $J = L + S$ is the total moment and μ_{eff} is the effective paramagnetic moment. We can determine the effect of paramagnetic moment (μ_{eff}^{exp}) from the curie constant. The theoretical μ_{eff}^{calc} is estimated using the following expression:

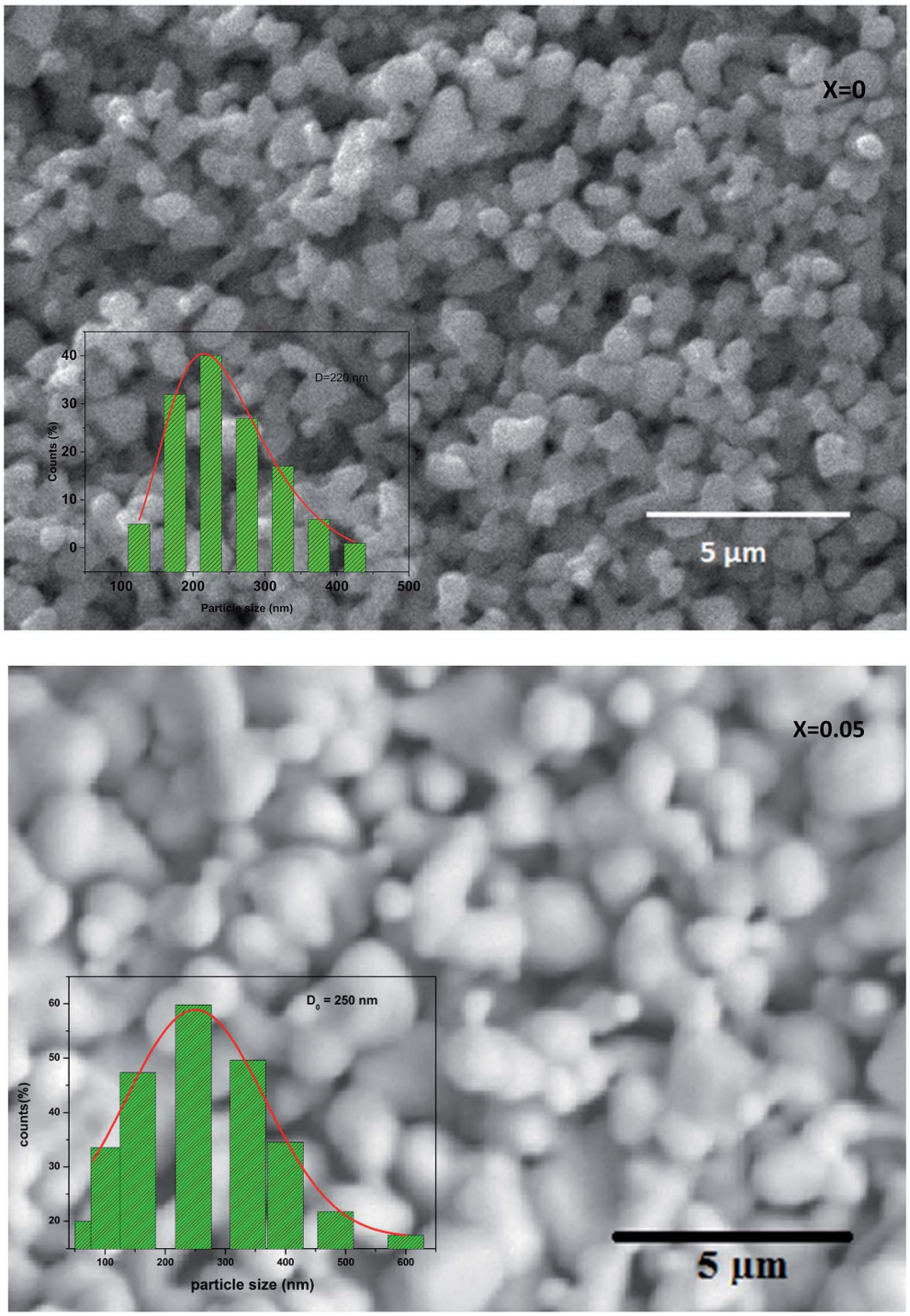

Fig. 3 Scanning electron micrograph for $La_{0.67-x}Bi_xBa_{0.33}MnO_3$ ($x = 0$ and 0.05) manganite. The inset: dispersion histogram.

$\mu_{eff}^{calc} = \sqrt{0.67\mu_{eff}{}^2(Mn^{3+} = 4.9\mu_B) + 0.33\mu_{eff}{}^2(Mn^{4+} = 3.87\mu_B)}$. The parameters μ_{eff}^{exp} and μ_{eff}^{calc} are summarized in Table 2. It is found that the μ_{eff}^{exp} is greater as compared to μ_{eff}^{calc}. This discrepancy validates the formation of ferromagnetic spin clusters within the paramagnetic state.[19] A linear fit yields positive Curie–Weiss temperature $\theta_{CW} = 312$ K ($x = 0.05$). This result confirms a mean FM interaction between spins for all samples (Table 2). Moreover, this value is higher than T_C, which may be due to the existence of short range FM ordering.[19]

The structure analysis shows that the unit cell becomes slightly larger as the $6s^2$ lone pair character becomes dominant, it has been shown that the Bi–O bond is shorter than the La–O, despite of the similar ionic radius of La^{3+} and Bi^{3+} ions.[20] This can be interpreted as arising from the rather covalent character of the Bi–O bonds. The electronegativity of Bi enhances

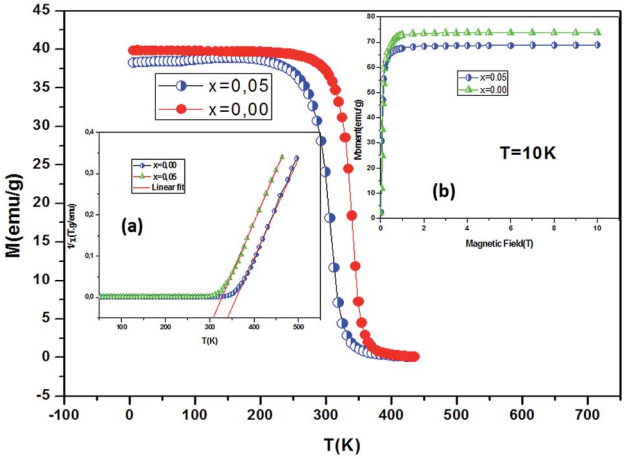

Fig. 4 Temperature dependence of the magnetization measured at $\mu_0 H = 0.05$ T for $La_{0.67-x}Bi_xBa_{0.33}MnO_3$ sample ($x = 0$ and 0.05). Inset (a) show temperature dependence of the inverse dc magnetic susceptibility from magnetization measurements. Inset (b) variation of the magnetization as a function of applied magnetic field at 10 K.

hybridisation between $6s^2$ of Bi^{3+} orbitals and 2p of O^{2-} orbitals and this hybridisation produces a local distortion. It is observed that transition temperature T_C decreases with increase in Bi ratio. This is presumably due to tilts the MnO_6 octahedra, resulting in a reduced overlap between the Mn-3d and O-2p orbitals.[21] It should also be noted that the $La_{0.67}Ba_{0.33}MnO_3$ sample is ferromagnetic while $Bi_{0.67}Ba_{0.33}MnO_3$ is antiferromagnetic, indicating a competition between the double exchange and the antiferromagnetic super exchange in these compounds can decrease T_C. This phenomenon has been observed in the compound $Bi_{0.6-x}La_xCa_{0.4}MnO_3$.[22]

3.3 Effect of Bi on magnetocaloric properties

The change of magnetic entropy of magnetic compounds has the largest value near a phase transition. According to the classical thermodynamic theory, the isothermal magnetic entropy change ($-\Delta S_M$) produced by the variation of a magnetic field from zero to $\mu_0 H_{max}$ is given by:[23,24]

$$\Delta S_M(T, \mu_0 H) = S_M(T, \mu_0 H) - S_M(T, 0) = \int_0^{\mu_0 H_{max}} \left(\frac{\partial S}{\partial(\mu_0 H)}\right)_T \mathrm{d}(\mu_0 H)$$

The magnetic entropy is related to the magnetization M, magnetic field strength $\mu_0 H$ and absolute temperature T through the Maxwell relation:

$$\left(\frac{\partial S}{\partial(\mu_0 H)}\right)_T = \left(\frac{\partial M}{\partial T}\right)_{\mu_0 H}$$

In the case of magnetization measurement in small discrete magnetic fields and temperature interval ΔT, ΔS_M can be approximated to:

$$\Delta S_M\left(\frac{T_1 + T_2}{2}\right) = \left(\frac{1}{T_2 - T_1}\right)\left[\int_0^{\mu_0 H_{max}} M(T_2, \mu_0 H)\mathrm{d}(\mu_0 H) - \int_0^{\mu_0 H_{max}} M(T_1, \mu_0 H)\mathrm{d}(\mu_0 H)\right]$$

The $-\Delta S_M(T)$ data calculated from the $M(\mu_0 H)$ curves (inset in Fig. 5) at different magnetic fields for the $La_{0.67-x}Bi_xBa_{0.33}MnO_3$ ($x = 0$ and 0.05) are plotted in Fig. 5. The compounds exhibit large changes in magnetic entropy around Curie temperature (T_C), which is a characteristic property of simple ferromagnets due to the efficient ordering of magnetic spins at the temperature induced by magnetic field.[25] Large magnetic entropy changes ΔS_M^{max} are reported for all the samples and are summarized in Table 3. The magnitude of $(-\Delta S_M^{max}(T))$ for all samples increases with increasing the applied magnetic field (inset of Fig. 5). For example, the maximum magnetic-entropy value increases from 2.37 J kg^{-1} K^{-1} for $x = 0.00$ to 2.8 J kg^{-1} K^{-1} (2T) and 5.8 J kg^{-1} K^{-1} for $x = 0.00$ to 7.3 J kg^{-1} K^{-1} for $x =$

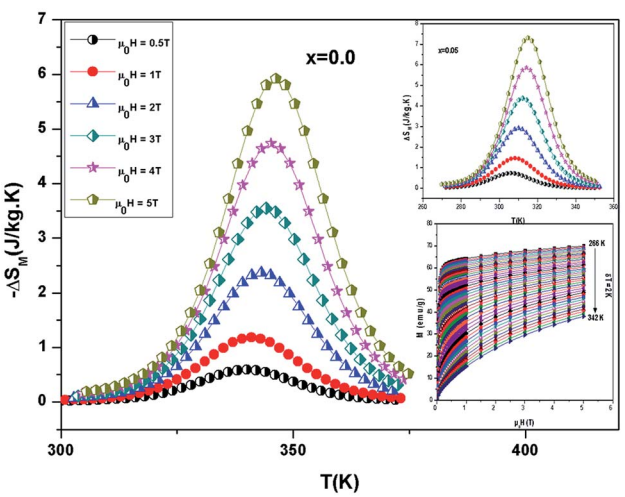

Fig. 5 Temperature dependence of magnetic entropy change under different external fields for $La_{0.67-x}Bi_xBa_{0.33}MnO_3$ samples. Inset: magnetization *versus* applied magnetic field $\mu_0 H$, measured at different temperatures, for example the sample $La_{0.62}Bi_{0.05}Ba_{0.33}MnO_3$.

Table 2 Transition temperature T_C, W/W_0 and Curie Weiss temperature θ_W as a function of x content for $La_{1-x}Bi_xBa_{0.33}MnO_3$ samples

x	T_C (K)	W/W_0 (10^{-2})	θ_{CW} (K)	$\theta_{Mn-O-Mn}$ (°)	d_{Mn-O} (Å)	μ_{eff}^{exp} (μ_B)	μ_{eff}^{calc} (μ_B)
0	340	4.73	348	165.32	1.959	5.32	4.586
0.05	306	4.66	312	165.12	1.965	5.81	4.586

Table 3 ΔS_M and RCP values for the present samples and for some previous works

Composition	T_C (K)	$(-\Delta S_M^{max})$ (J kg^{-1} K^{-1})	RCP (J kg^{-1})	$\mu_0 H$ (T)	Ref.
$Gd_5(Sr_2Ge_2)$	275	18.5	535	5	24
Gd	294	10.2	410	5	25
$La_{0.5}Sm_{0.1}Sr_{0.4}Mn_{0.95}In_{0.05}O_3$	308	4.50	193.48	5	26
$La_{0.67}Sr_{0.33}Mn_{0.9}Cr_{0.1}O_3$	328	5	—	5	27
$La_{0.67}Ba_{0.33}MnO_3$	346	5.80	151	5	This work
$La_{0.62}Bi_{0.05}Ba_{0.33}MnO_3$	310	7.30	209	5	This work
Gd	297	4	120	2	28
$MnFeP_{0.45}As_{0.5}$	300	14.5	188	2	28
$La_{0.7}Sr_{0.3}Mn_{0.95}Ti_{0.05}O_3$	308	2.2	90	2	29
$La_{0.7}Sr_{0.3}Mn_{0.9}Fe_{0.1}O_3$	260	1.7	83	2	30
$La_{0.67}Ba_{0.33}MnO_3$	343	2.37	39	2	This work
$La_{0.62}Bi_{0.05}Ba_{0.33}MnO_3$	308	2.80	80	2	This work

0.05 respectively (5T). Guo *et al.*[26] indicated that the large magnetic entropy change in perovskite compounds could originate from the spin–lattice coupling in the magnetic ordering process. Strong coupling between spin and lattice is corroborated by the observed significant lattice change accompanying magnetic transition in perovskite manganites.[27] The lattice structural change in the Mn–O bond distance as well as in the ⟨Mn–O–Mn⟩ bond angle would in turn favor the spin ordering. Thus a more abrupt variation of magnetization near Curie temperature (T_C) occurs, resulting in a large magnetic entropy change as a large MCE.

The change of magnetic entropy can be also calculated from the field dependence of the specific heat by the following integration:

$$\Delta S_M(\mu_0 H,\ T) = \int_0^T \frac{C_p(\mu_0 H,\ T) - C_p(0, T)}{T} dT$$

From this equation, it determine the change of specific heat induced by the external magnetic field zero to $\mu_0 H$ as: $\Delta C_p(\mu_0 H,\ T) = C_p(\mu_0 H,\ T) - C_p(0,\ T) = T\frac{\partial \Delta S_M(\mu_0 H,\ T)}{\partial T}$.

Fig. 6 shows the temperature dependence of $\Delta C_p(\mu_0 H,\ T)$ under different field variations for the samples (for example $x = 0.05$) calculated from the $\Delta S_M(\mu_0 H,\ T)$. The $\Delta C_p(\mu_0 H,\ T)$ undergoes a sudden change from positive to negative around T_C with a positive value above T_C and a negative value below T_C. The maximum/minimum value of $\Delta C_p(\mu_0 H, T)$ observed at 320/300 K, exhibits an increasing trend with applied field and is obtained to be 122.4/−115.43 J kg^{-1} K^{-1} for $x = 0.05$ at 5 T.

It should be noted that $(-\Delta S_M^{max})$ is not the only parameter deciding about an applicability of material. To estimate if a material can be a good candidate for magnetic refrigeration (MR), Gschneidner and Pecharsky[28] defined the relative cooling power (RCPS), which is the important index which is used to evaluate the cooling efficiency of a magnetic refrigerant. It is defined as the product between the maximum values of the magnetic entropy change $(-\Delta S_M^{max})$ and the full width at half maximum δT_{FWHM} of the magnetic entropy change curve (RCP(S) $= -\Delta S_M^{max} \times \delta T_{FWHM}$).[29] This parameter corresponds to the amount of heat that can be transferred between the cold and hot parts of the refrigerator in one ideal thermodynamic cycle. The results are summarized in Table 3. Fig. 7 shows the

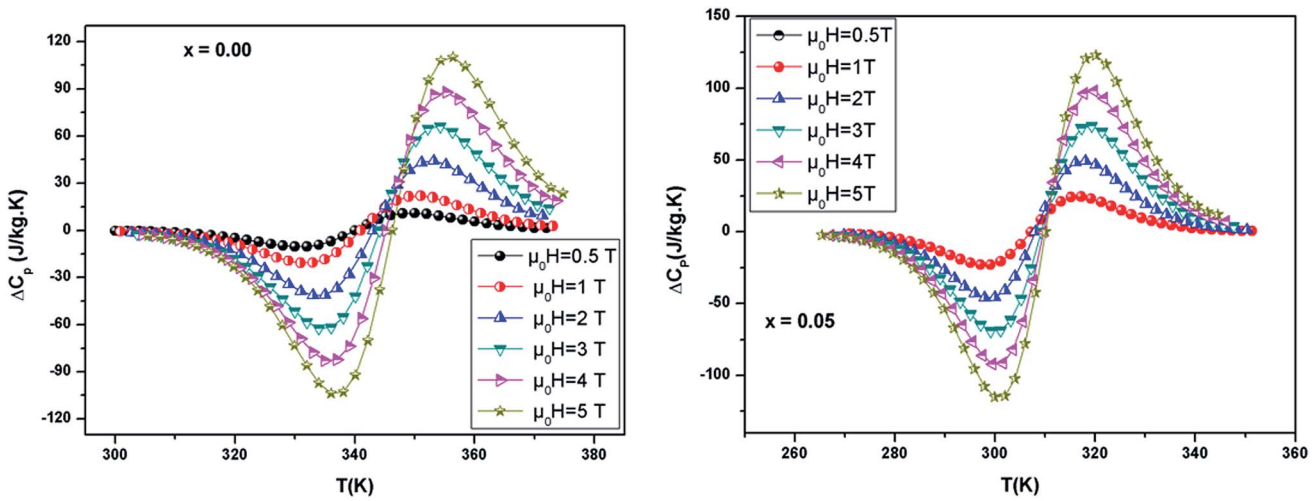

Fig. 6 Change of specific heat of the samples as a function of temperature at different magnetic field.

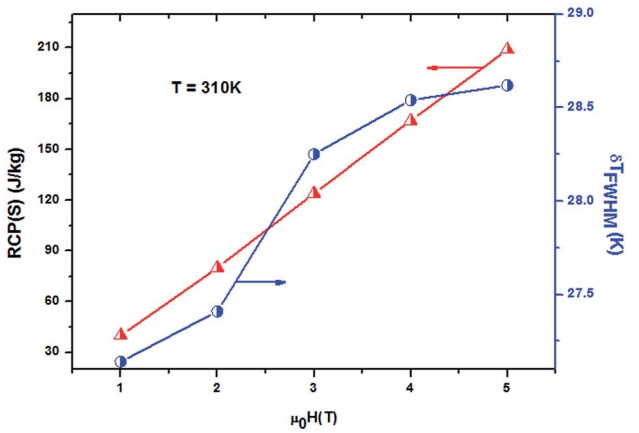

Fig. 7 Magnetic field dependence of RCP and δT_{FWHM} at 310 K for $x =$ 0.05 for example.

absolute value of RCPS and δT_{FWHM} for the sample ($x = 0.05$) *versus* applied field at 310 K. It can be seen from this figure that RCPS (δT_{FWHM}) increases monotonically as the field increases. The value of RCP is about 51% of Gd at 294 K for $\mu_0 H = 5$ T.[30] To evaluate the applicability of ours samples as a magnetic refrigerant, the obtained values of ΔS_M in our study are compared in Table 3 with those reported in the literature for several other magnetic compounds.[31–37]

3.4 Modeling the magnetic properties

The Weiss molecular mean field model is a standard model in magnetism. Because of its simplicity, this model is still used in current research for a wide range of magnetic materials, although its limitations are well known. This concept of a molecular field assumes that the magnetic interaction between magnetic moments is equivalent to the existence of an exchange interaction depending on the magnetization M:[38]

$$H_{eff} = H + H_{exch} = H + \lambda M$$

where H and H_{exch} are the external magnetic field, the exchange magnetic field and λ the mean field exchange parameter respectively.

Amaral *et al.* proposed a model based on mean field theory and presented an approach of applying this method scenario to isotherm magnetization $M(T, H)$ measurements.[39] In our study, it consider the general mean field law:[40] $M(H, T) = B_J[(H + H_{exch})/T]$, the Brillouin function B_J is written as: $B_J(X) = \frac{2J+1}{2J}\coth\left[\frac{(2J+1)X}{2J}\right] - \frac{1}{2J}\coth\left(\frac{X}{2J}\right)$, where $X = \frac{Jg\mu_B H_{eff}}{k_B T}$, J is the total angular momentum in the lattice, g is the gyromagnetic factor (landé factor), μ_B is the Bohr magnetron and k_B is the Boltzmann's constant. The mean field exchange parameter λ is not predetermined. Then for corresponding values with the same $(H + H_{exch})/T$, M is also the same, the value of the inverse $B_J^{-1}(M)$ function,[41]

$$\frac{H}{T} = B_J^{-1}(M) - \frac{H_{exch}}{T}$$

The study of the exchange field induced by the magnetization change makes it possible to find the value of the average field exchange parameter λ. Fig. 8 shows H/T *versus* $1/T$ for some of the values of M (5 emu per g per step) from 266 K to 342 K for $x =$ 0.05. According to the mean scaling method such H/T *versus* $1/T$ curves should show a series of straight lines at different temperature. The linear relationship between H/T and $1/T$ is kept. Linear fits are then easily made to each isomagnetic line. Typically, the interpolation step was of 1 emu g^{-1}. The slope of this isomagnetic line, will then give the exchange field (H_{exch}).

For all compounds in the paramagnetic domain or the materials of domain ordered such as anti-ferromagnetic, it can always expand increasing M in powers of H, or H in powers of M. In this latter approach it stop at the third order and considering that the magnetization is an odd function of field, it can write:[42]

$$H_{exch} = \lambda_1 M + \lambda_3 M^3$$

Fig. 9 shows the evolution of the exchange field *versus* the magnetization for the $La_{0.67-x}Bi_xBa_{0.33}MnO_3$ ($x = 0.05$ for example). The experimental data should be included for the fit by eqn ($H_{exch} = \lambda_1 M + \lambda_3 M^3$). The results show a very small dependence on M^3 ($\lambda_3 = -1.3984 \times 10^{-5}$ (T g emu^{-1})^3), is found for this second order transition system, thus $H_{exch} = \lambda_1 M$ with $\lambda_1 = 1.25$ T g emu^{-1}. After obtaining the mean field exchange parameter the next step of this method consists on building the scaling plot of M *vs.* $(H + H_{exch})/T$ (Fig. 10). It has successfully fitted the scaled magnetization data with the Brillouin function. From the scaling plot and the subsequent fit with the saturation magnetization equal to 72 emu g^{-1} (this value is close to the experimental one ($M_s = 69$ emu g^{-1} at 10 K) (inset b of Fig. 4), and the value of the total angular momentum of the manganite is $J = 1.9$.

The magnetization measurements in the law temperature range show that the saturation magnetization is about $M_s^{theor} = Jg\mu_B = 3.67\mu_B$/f.u. This value is close to the experimental value $M_s^{exper} = 3.7\mu_B$ at 10 K. The value of M_s^{theor} per formula unit is given by: $M_s^{theor} = (n_{Mn^{3+}})M_{sMn^{3+}} + (n_{Mn^{4+}})M_{sMn^{4+}}$, where $M_{sMn^{3+}} =$

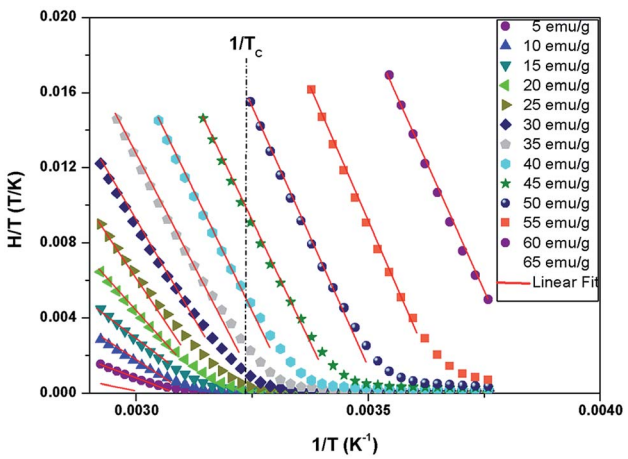

Fig. 8 H/T *versus* $1/T$ curves with constant values of magnetization per curve for $La_{0.62}Bi_{0.05}Ba_{0.33}MnO_3$ compound.

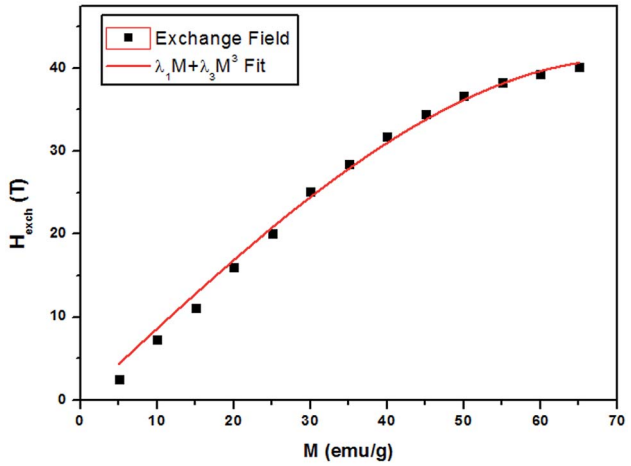

Fig. 9 Exchange field *versus* magnetization for $La_{0.62}Bi_{0.05}Ba_{0.33}MnO_3$ sample, with the function $\lambda_1 M + \lambda_3 M^3$ fit.

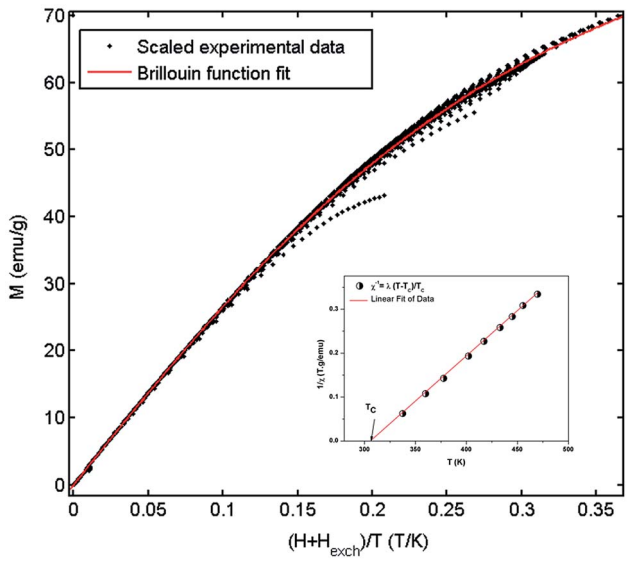

Fig. 10 Mean-field scaling plot and Brillouin function fit. Inset $1/\chi$ *versus* T of $La_{0.62}Bi_{0.05}Ba_{0.33}MnO_3$ compound.

$4\mu_B$ and $M_{sMn^{4+}} = 3\mu_B$ are the magnetic moments, $n_{Mn^{3+}} = 0.67$ and $n_{Mn^{4+}} = 0.33$ are the contents of Mn^{3+} and Mn^{4+} ions respectively. It deduce that the total angular momentum of the compound is $J = 1.835$ (it was assumed that $g = 2$).

From a linear approximation of the susceptibility (Curie law) : $\frac{\mu_0 M}{H} = \frac{1}{\lambda}\frac{T_C}{T - T_C}$. Inset of the Fig. 10 shows the evolution of the inverse susceptibility $(1/\chi)$ *versus* temperature for the $La_{0.62}Bi_{0.05}Ba_{0.33}MnO_3$ compound. The straight line represents the Curie–Weiss law with $\lambda = 1.25$ T g emu^{-1} and $T_C = 306$ K. The intersection is obtained at a temperature value equals to the critical one. At this point, the susceptibility becomes infinite, which corresponds to the ferromagnetic–paramagnetic transition. Fig. 11 shows how experimental data can be described using the mean-field method. A good

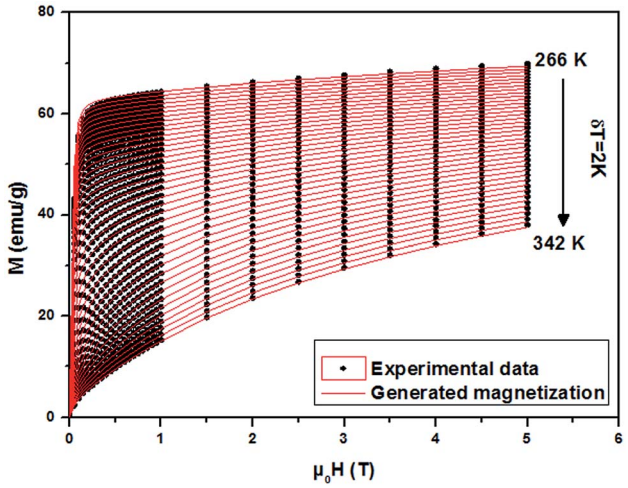

Fig. 11 Experimental magnetization *versus* $\mu_0 H$ (black symbols) of $La_{0.62}Bi_{0.05}Ba_{0.33}MnO_3$ sample and the interpolation using the mean field method (red lines).

agreement between the experimental $M(T, \mu_0 H)$ curves and the mean-field generated curves with the obtained parameters, except near the paramagnetic-ferromagnetic transition (T_C), which are not adequately described. This result is probably due to the formation of magnetic domains and critical effects.

3.5 Estimating the magnetocaloric effect (MCE)

The mean field approach allows us to estimate magnetic entropy variation ΔS_M within the thermodynamics of the model and without using the usual numerical integration of a Maxwell relation.[43] Within the mean field approach, ΔS_M between magnetic fields H_1 and H_2 can be calculated using the following general expression, which also accounts for a possible dependence of λ on T:

$$-\Delta S_M(T) = \int_{\frac{H_1}{M}}^{\frac{H_2}{M}} \left[B_J^{-1}(M) - \frac{\partial \lambda}{\partial T} M \right] dM$$

The linearity relation between H/T and $1/T$ in Fig. 8 improves that the mean field exchange parameter λ is independent of the temperature T. So the following equation will be simplified:

$$-\Delta S_M(T) = \int_{\frac{H_1}{M}}^{\frac{H_2}{M}} B_J^{-1}(M) dM$$

Fig. 12 shows the evolution of the magnetic entropy change $(-\Delta S_M)$ data as a function of temperature at several magnetic applied fields for the $La_{0.62}Bi_{0.05}Ba_{0.33}MnO_3$ compound, by using the Maxwell relation and that basing on mean field theory. Both results are in good agreement, except close to T_C, here an excepted small difference appears, due to the formation of magnetic domains and critical effects.

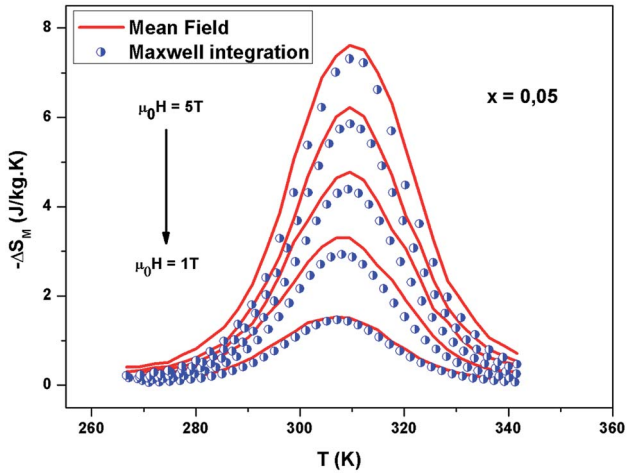

Fig. 12 Experimental and calculated magnetic entropy as a function of temperature for $x = 0.05$.

4 Conclusion

In summary, single phase $La_{0.67-x}Bi_xBa_{0.33}MnO_3$ ($x = 0.00$ and 0.05) compounds were prepared by the sol–gel technic. Using the magnetization measurements, magnetic and magneto-caloric effect have been studied. These compounds show second order ferromagnetic–paramagnetic phase transition, with a large magnetic entropy change. It have studied the mean-field scaling method for these samples. The insight that can be gained from the use of this methodology for a given magnetic system can be of great interest. In a simplistic approach, it can say that if this scaling method does not follow a molecular mean-field behavior, other methods must be pursued in order to interpret the magnetic behavior of the system. The mean-field scaling method is able to determine the exchange parameters J, λ and g of ours samples. These factors allow estimating some magnetic properties.

Conflicts of interest

There are no conflicts to declare.

References

1 M. Khlifi, E. Dhahri and E. K. Hlil, *J. Alloys Compd.*, 2014, **587**, 771–777.
2 G. F. Wang, L. R. Li, Z. R. Zhao, X. Q. Yu and X. F. Zhang, *Ceram. Int.*, 2014, **40**, 16449–16454.
3 E. Dagotto, T. Hotta and A. Moreo, *Phys. Rep.*, 2001, **344**, 1.
4 A. Dhahri, E. Dhahri and E. K. Hlil, *J. Alloys Compd.*, 2017, **700**, 169–174.
5 R. Von Helmolt, J. Wecker, B. Holzapfel, L. Schultz and K. Samwer, *Phys. Rev. Lett.*, 1993, **71**, 2331.
6 C. P. Bean and D. S. Rodbell, *Phys. Rev.*, 1962, **126**, 104–115; D. Rodbell, *Phys. Rev. Lett.*, 1961, **7**, 1.
7 G. Lalitha and P. Venugopal Reddy, *J. Alloys Compd.*, 2010, **494**, 476–482.
8 J. Rodriguez Carvajal, *FULLPROF*, Laboratoire Leon Brillouin (CEACNRS), 2000–2005.
9 A. M. Glazer, *Acta Crystallogr.*, 1972, **B28**, 3384.
10 V. M. Goldschmidt, *Geochemistry*, Oxford University Press, 1958, p. 730.
11 R. D. Shannon, *Acta Crystallogr.*, 1976, **A32**, 751.
12 G. Lalitha and P. Venugopal Reddy, *J. Alloys Compd.*, 2010, **494**, 476–482.
13 G. K. Williamson and W. H. Hall, *Acta Metall.*, 1953, **1**, 22–31.
14 A. G. Mohamed, S. Ghodhbane, A. Dhahri, J. Dhahri and E. K. Hlil, *J. Alloys Compd.*, 2016, **681**, 547–554.
15 B. Aslibeiki, P. Kameli and M. H. Ehsani, *Ceram. Int.*, 2016, **42**, 12789–12795.
16 C. Lavorato, E. Lima Jr, D. Tobia, D. Fiorani, H. E. Troiani, R. D. Zysler and E. L. Winkler, *Nanotechnology*, 2014, **25**, 355704.
17 F. Sugawara, S. Iida, Y. Syono and S. Akimoto, *J. Phys. Soc. Jpn.*, 1968, **25**, 1553.
18 N. A. Hill and K. M. Rabe, *Phys. Rev. B: Condens. Matter Mater. Phys.*, 1999, **59**, 8759.
19 A. Dhahri, M. Jemmali, K. Taibi, E. Dhahri and E. K. Hlil, *J. Alloys Compd.*, 2015, **618**, 488–496.
20 M. Barandiarana, J. Gutierrez, L. Righi, M. Amboage, A. Pena, T. Hernandez, M. Insausti and T. Rojo, *Physica B*, 2001, **299**, 286–292.
21 *Colossal magneto-resistance oxides*, ed. Y. Tokura, Gordon and Breach, London, 2000.
22 R. R. Zhang, G. L. Kuang, L. H. Yin and Y. P. Sun, *J. Appl. Phys.*, 2010, **108**, 103903.
23 M. Dhahri, A. Zaidi, K. Cherif, J. Dhahri and E. K. Hlil, *J. Alloys Compd.*, 2017, **715**, 266–274.
24 Ah. Dhahri, E. Dhahri and E. K. Hlil, *Appl. Phys. A*, 2014, **116**, 2077–2085.
25 A. Bhattacharyya, S. Chatterjee, S. Giri and S. Majumdar, *Eur. Phys. J. B*, 2009, **70**, 347.
26 Z. B. Guo, Y. M. Du, J. S. Zhu, H. Huang, W. P. Ding and D. Feng, *Phys. Rev. Lett.*, 1997, **78**, 1142.
27 P. G. Radaelli, D. E. Cox, M. Marezio, S. W. Cheong, P. E. Schiffer and A. P. Ramirez, *Phys. Rev. Lett.*, 1995, **75**, 4488.
28 V. K. Pecharsky and K. A. Gschneidner Jr, *J. Appl. Phys.*, 1999, **86**, 565.
29 E. L. T. França, A. O. dos Santos, A. A. Coelho and L. M. da Silva, *J. Magn. Magn. Mater.*, 2016, **401**, 1088–1092.
30 V. K. Pecharsky, K. A. Gschneidner and A. O. Tsokol, *Rep. Prog. Phys.*, 2005, **68**, 1479.
31 K. A. Gschneidner Jr, V. K. Pecharsky and A. O. Tsokol, *Rep. Prog. Phys.*, 2005, **68**, 1479.
32 M. H. Phan and S. C. Yu, *Magn. Magn. Mater.*, 2007, **308**, 325.
33 M. Dhahri, A. Zaidi, K. Cherif, J. Dhahri and E. K. Hlil, *J. Alloys Compd.*, 2017, **691**, 578–586.
34 Y. Sun, W. Tong and Y. Zhang, *J. Magn. Magn. Mater.*, 2001, **232**, 205–208.
35 O. Tegus, E. Bruck, K. H. J. Buschow and F. R. de Boer, *Nature*, 2002, **415**, 150.

36 D. N. H. Nam, N. V. Dai, L. V. Hong, N. X. Phuc, S. C. Yu, M. Tachibana and E. Takayama Muromachi, *J. Appl. Phys.*, 2008, **103**, 043905.
37 S. K. Barik, C. Krishnamoorthi and R. Mahendiran, *J. Magn. Magn. Mater.*, 2011, **323**, 1015e1021.
38 A. Arrott, *J. Appl. Phys.*, 2008, **103**, 07C715.
39 J. Amaral, N. Silva and V. Amaral, *Appl. Phys. Lett.*, 2007, **91**, 172503e172503.
40 A. M. Tishin and Y. I. Spichkin, *The Magnetocaloric Effect and its Applications*, IOP Publishing, 2003, Bristol.
41 J. Amaral, N. Silva and V. Amaral, *Appl. Phys. Lett.*, 2007, **91**, 172503e172503.
42 M. Cyrot, *et al.*, *Magnétisme I-Fondement*, Presses universitaires de Grenoble, Grenoble, 1999.
43 Ah. Dhahri, M. Jemmali, K. Taibi, E. Dhahri and E. K. Hlil, *J. Alloys Compd.*, 2015, **618**, 488–496.